Supplementary Information

A New Adsorption Energy-Barrier Relation and Its Application to CO_2 Hydrogenation to Methanol over In_2O_3-Supported Metal Catalysts

Deshuai Yang,[1,2] Huili Lu,[1] Guixiang Zeng,[*2] Zhao-Xu Chen,[*1]

[1]*Institute of Theoretical and Computational Chemistry, School of Chemistry and Chemical Engineering, Nanjing University, Nanjing 210023, People's Republic of China*

[2]*Kuang Yaming Honors School and Institute for Brain Sciences, Nanjing University, Nanjing 210023, People's Republic of China*

E-mail: zxchen@nju.edu.cn; gxzeng@nju.edu.cn

Models and Computational Methodology:

The In_2O_3-supported metal catalysts were modeled with M_4/In_2O_3 (110)[S1] (M= Ni, Ag, Pt, Rh, Ir and Pd) (Fig. S1a-f). The In_2O_3 (110) surface was modeled with a four-layer slab of $(1\times\sqrt{2})$ surface unit cell constructed from the optimized cubic bulk In_2O_3 with the lattice parameter of 10.22 Å, which is in agreement with the experimental result.[S2] A vacuum of ~14 Å was adopted and the cell has a dimension of 10.22 Å × 14.45 Å × 20.00 Å, consisting of 32 Indium atoms and 48 Oxygen atoms.

All DFT calculations were carried out using the Vienna *Ab initio* Simulation Package (VASP).[S3] The projector-augment wave (PAW) method[S4] and Generalized gradient approximation (GGA) with Perdew-Burke-Ernzerhoff (PBE) functional[S5] were employed to describe the electron-ion interaction and exchange-correlation interaction, respectively. The plane-wave energy cutoff was set to 400 eV and DFT-D3 method[S6] implemented in VASP was adopted to evaluate the Van der Waals (vdW) interaction. The Brillouin zone was sampled using a (2×2×1) k-point grid according to the Monkhorst Pack method.[S7] Test calculations of CO_2 adsorption energy on Ni_4/In_2O_3(110) indicate that the error with 400 eV cutoff energy and (2×2×1) k-point is within chemical accuracy (1 kcal/mol). Spin-polarized effects were considered. Geometry optimization was stopped when the force on each relaxed atom is no more than 0.02 eV/Å. The transition states (TSs) were located using the climbing image nudged elastic band (CI-NEB) method.[S8] All the located stationary points are characterized by frequency analysis with each transition state has one and only one imaginary frequency along the reaction coordinate, and initial and final states have no imaginary frequencies.

Microkinetics modeling:

For surface reactions, the forward and backward rate constants were determined used the Eyring equation: [S9]

$$k = \frac{k_b T}{h} \frac{Q_T}{Q} e^{-E_a/k_b T} \quad (1)$$

Where k is the reaction rate constants (in s^{-1}), k_b and h are the Boltzmann and Planck's constants, respectively. T and E_a are the reaction temperature (in K) and energy barrier, respectively. Q_T and Q are the partition function of the transition state and initial or final state, respectively.

For the molecular adsorption, we assumed that the molecule loses one of its translational degrees of freedom with respect to the gas phase. The changes of the rotational degree of freedom were neglected. Then, the adsorption rate constant k_{ads} was calculated as: [S10]

$$k_{ads} = \frac{PA'}{\sqrt{2\pi m k_b T}} S \quad (2)$$

Where P indicates the partial pressure of the adsorbate in the gas phase, A' refers to the surface area of the adsorption site, S and m represent the sticking coefficient and the mass of the adsorbate, respectively. The sticking coefficients for CO_2 and H_2 were set to 1.

For the desorption process, we assumed that the activated complex has three rotational degree of freedom and two translation degree of freedom. According, the desorption rate constant k_{ads} can be defined as:[S10]

$$k_{des} = \frac{k_b T^3}{h^3} \frac{A'(2\pi m k_b)}{\sigma \theta_{rot}} e^{-E_{des}/k_b T} \quad (3)$$

Where σ and θ represent the symmetry number and the characteristic temperature for rotation, respectively. E_{des} is the desorption energy.

Different equations for all surface reaction species were constructed by using the rate constants of the elementary reaction steps. For each of the X components involved in the reaction network, a single differential equation is defined as:

$$r_i = \sum_{j=1}^{N} \left(k_j v_i^j \prod_{k=1}^{X} c_k^{v_k^j} \right) \quad (4)$$

Where k_j is the elementary reaction rate constant, v_i^j is the stoichiometric coefficient of component i in elementary step k, and c_k refers to the concentration of component k on catalyst surface.

To identify the rate-determining step of the CO_2 hydrogenation reaction, Campbell´s degree of rate control (DRC) analysis was employed.[S11] To a specific elementary step i, the DRC coefficient ($\chi_{RC,i}$) is defined as:

$$\chi_{RC,i} = \frac{k_i}{r} \left(\frac{\partial r}{\partial k_i} \right)_{k_{j \neq i}, K_i} = \left(\frac{\partial \ln r}{\partial \ln k_i} \right)_{k_{j \neq i}, K_i} \quad (5)$$

Where k_i, K_i and r refer to the rate constant, equilibrium constant for step i, and the overall reaction rate, respectively. A positive value of $\chi_{RC,i}$ indicates a rate-controlling step, while a negative value indicates inhibition. Additionally, DRC coefficients obey the sum rule and the sum of all $\chi_{\mathrm{RC,i}}$ values equals to unity.

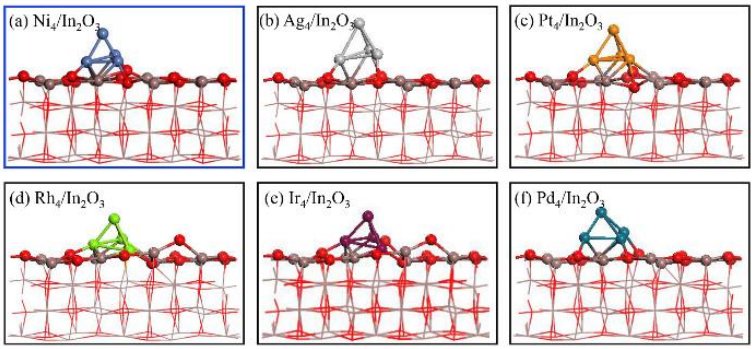

Fig. S1 Optimized structures of (a) Ni_4/In_2O_3(110), (b) Ag_4/In_2O_3(110), (c) Pt_4/In_2O_3(110), (d) Rh_4/In_2O_3(110), (e) Ir_4/In_2O_3(110) and (g) Pd_4/In_2O_3(110). Red, O atoms; Brown, In atoms; Blue, Ni atoms; Gray, Ag atoms; Orange, Pt atoms; Green, Rh atoms; Purple, Ir atoms; Cyan, Pd atoms.

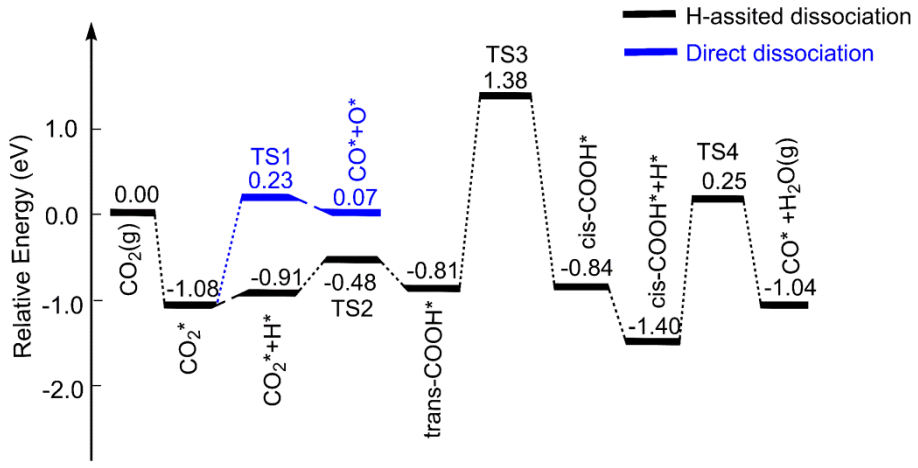

Fig. S2 Comparison of two routes of CO formation over Ni_4/In_2O_3(110) for the RWGS route.

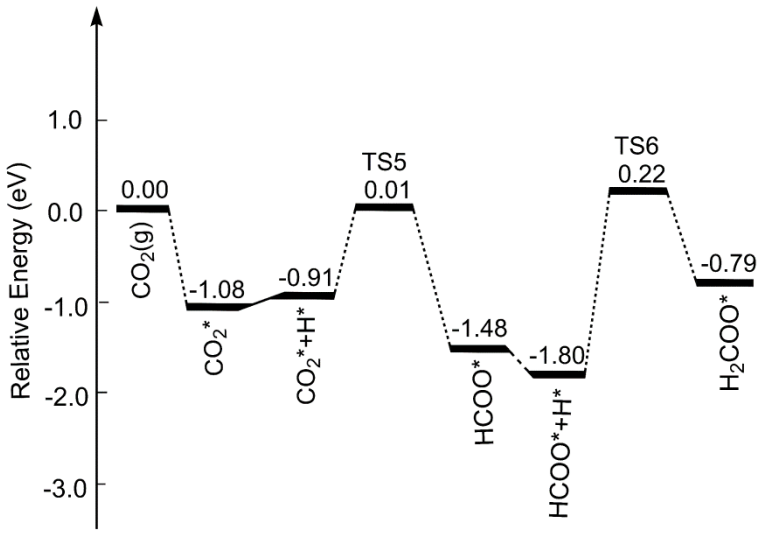

Fig. S3 Potential energy profiles of H_2COO over $Ni_4/In_2O_3(110)$ for the formate route.

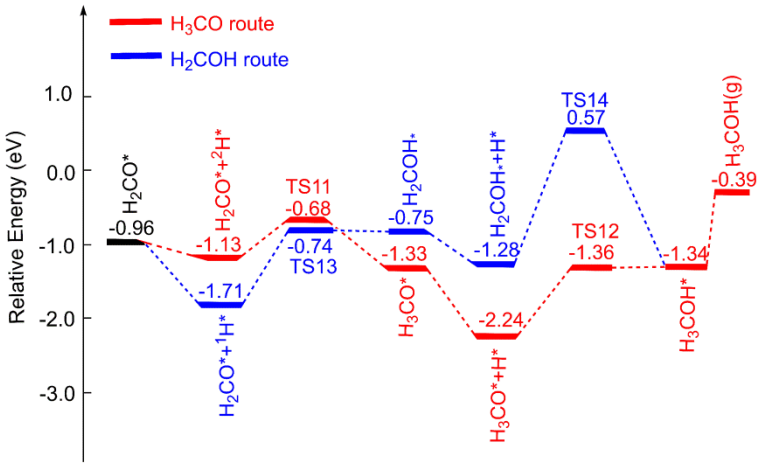

Fig. S4 Comparison of H_3CO and H_2COH routes for H_2CO* hydrogenation to methanol over $Ni_4/In_2O_3(110)$ for the formic acid (HCOOH) route.

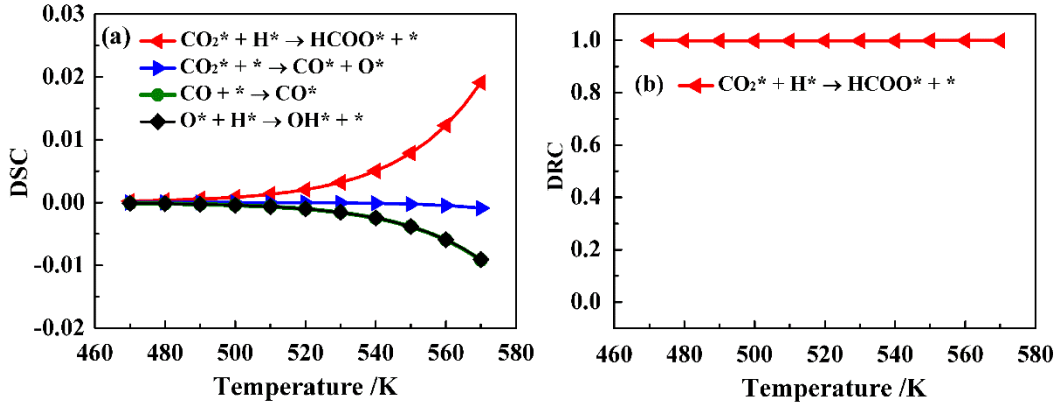

Fig. S5 Calculated (a) the degree of selectivity control (DSC) and (b) the degree of rate control (DRC) of methanol as a function of temperature based on microkinetic simulations (reaction conditions: CO_2:H_2 = 1:4, p = 50 bar).

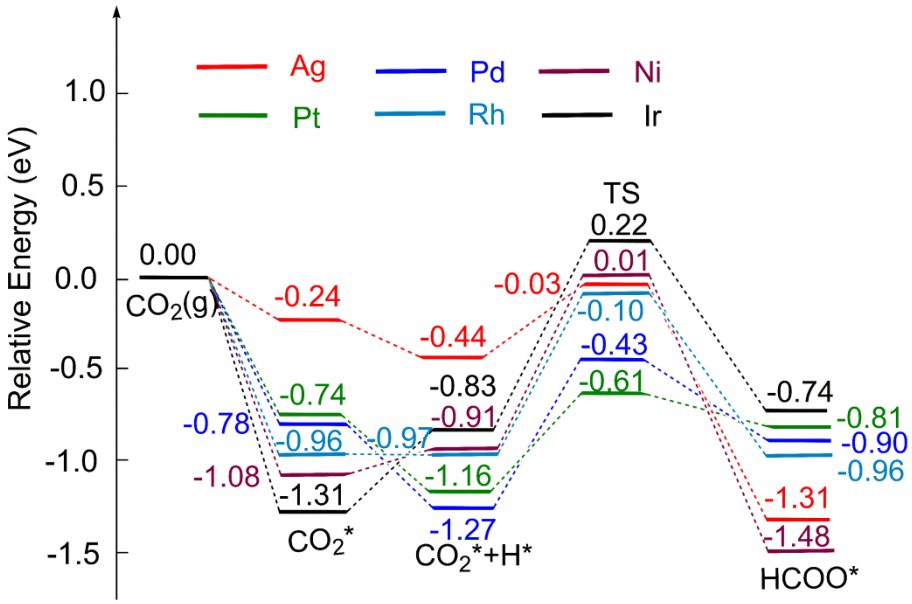

Fig. S6 Potential energy profiles for CO_2 hydrogenation to HCOO over $M_4/In_2O_3(110)$, where M = Ag, Pt, Pd, Rh, Ni and Ir.

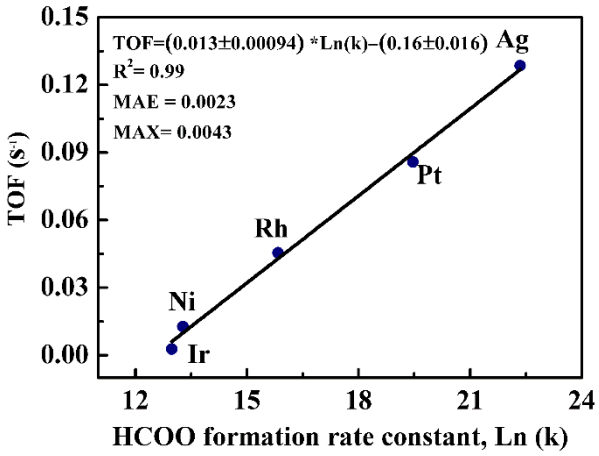

Fig. S7 Liner scaling correlation between logarithm of the HCOO formation rate constant, Ln(k), and the experimental turnover frequency (TOF) of methanol.

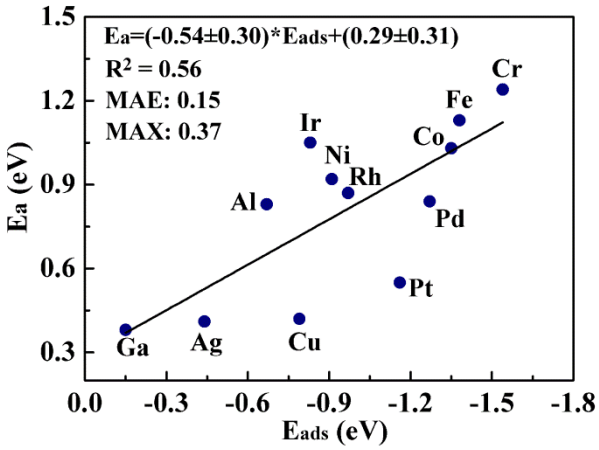

Fig. R8 Relationship between the co-adsorption energies (E_{ads}) of CO_2* + H* and the energy barriers (E_a) for CO_2 hydrogenation to HCOO step over In_2O_3 surface.

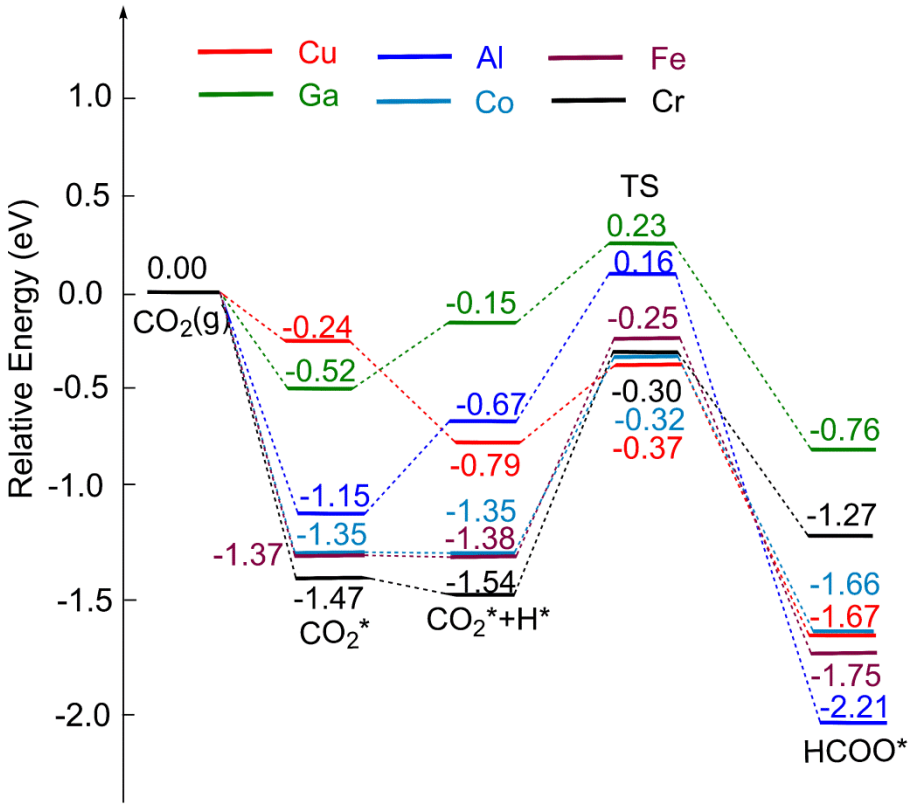

Fig. S9 Potential energy profiles for CO_2 hydrogenation to HCOO over $M_4/In_2O_3(110)$, where M = Cu, Ga, Al, Co, Fe and Cr.

Table S1. Calculated forward (E_f)/backward (E_b) energy barriers and the corresponding pre-exponential factors (A_f and A_r) of the elementary reactions involved in CO_2 hydrogenation to methanol over $Ni_4/In_2O_3(110)$. Pre-exponential factors are temperature dependent and are given here at a temperature of 300 ℃.

Elementary Step	Ni_4/In_2O_3			
	E_f (eV)	E_b (eV)	A_f (s^{-1})	A_b (s^{-1})
R1: CO_2* + * → CO* + O*	1.31	0.16	7.28E+13	8.50E+12
R2: CO_2* + H* → trans-COOH* + *	0.43	0.33	4.16E+12	7.31E+12
R3: trans-COOH* → cis-COOH*	2.19	2.22	3.86E+13	5.68E+13
R4: cis-COOH* + H* → CO* + H_2O*	1.65	1.29	1.13E+13	1.00E+14
R5: CO_2*+ H* → HCOO* + *	0.92	1.49	5.07E+13	1.59E+14
R6: HCOO* + H* → H_2COO* + *	2.02	1.01	4.80E+12	6.77E+12
R7: HCOO* + H* → HCOOH* + *	0.76	-0.02	1.68E+13	4.95E+12
R8: HCOOH* + * →HCO* + OH*	0.77	0.71	1.65E+12	1.40E+12
R9: HCO* + OH* + H* → HCO* + * + H_2O*	0.59	0.56	4.63E+12	3.96E+12
R10: HCO* + H* → H_2CO* + *	0.44	0.58	1.00E+13	6.31E+12
R11: H_2CO* + H* → H_3CO* + *	0.45	0.65	7.26E+12	1.24E+12
R12: H_3CO* + H*→ H_3COH* + *	0.88	-0.02	9.38E+11	2.83E+12
R13: H_2CO* + H* → H_2COH* + *	0.98	0.01	4.47E+12	2.71E+12
R14: H_2COH* + H* → H_3COH* + *	1.85	1.83	2.00E+13	2.97E+12

Table S2. Experimental turnover frequencies (TOFs) of methanol and relevant information for the six reported In_2O_3-supported metal catalysts for CO_2 hydrogenation to methanol.

Species	Metal loading (wt%)	Relative atomic mass (g/mol)	Space Time Yield of methanol STY, (g_{MeOH} g_{cat}^{-1} h^{-1})	TOF (s^{-1})	Ref
Ag	0.33	107.87	0.4530	1.29E-01	S12
Pd	0.97	106.42	0.8900	8.48E-02	S13
Rh	1.07	102.91	0.5448	4.55E-02	S14
Ir	10.00	192.22	0.7650	1.28E-02	S15
Ni	10.00	58.69	0.5500	2.80E-03	S16
Pt	1.07	195.08	0.5420	8.58E-02	S17

Table S3. Calculated forward energy barriers (E_f), pre-exponential factor (A_f) and reaction rate constant k_r for CO_2* + H* → HCOO* + * step over M_4/In_2O_3 (110), where M = Ag, Pt, Rh, Ni and Ir respectively. Pre-exponential factors and reaction rates are temperature dependent and are given here at a temperature of 300 ℃.

Species	E_f (eV)	A_f (s^{-1})	k_r(s^{-1})
Ag	0.40	1.78E+13	5.07E+09
Pt	0.54	1.75E+13	2.84E+08
Rh	0.87	3.48E+14	7.55E+06
Ni	0.92	5.07E+13	4.33E+05
Ir	1.05	1.04E+15	5.83E+05

Table S4. Calculated Bader charges (in unit |e|) and CO_2 adsorption energies (E_{ads}).

System	CO_2	O_1	O_2	C	M_t	M1	M2	M3	M4	In	E_{ads}
Ag	-0.03	-1.06	-1.10	2.12	0.71	0.24	0.24	0.01	0.22	1.54	-0.24
Pt	-0.58	-0.97	-1.06	1.45	0.54	0.20	0.09	0.14	0.11	1.62	-0.73
Pd	-0.55	-1.00	-1.07	1.52	0.64	0.23	0.09	0.19	0.14	1.62	-0.79
Rh	-0.64	-1.02	-1.08	1.46	0.90	0.28	0.18	0.22	0.21	1.62	-0.96
Ni	-0.70	-1.04	-1.07	1.41	1.11	0.34	0.27	0.27	0.24	1.62	-1.08
Ir	-0.53	-0.97	-1.11	1.55	0.71	0.23	0.13	0.18	0.18	1.60	-1.31
Cr	-0.96	-1.06	-1.08	1.18	2.18	0.59	0.53	0.50	0.56	1.61	-1.47
Co	-0.73	-1.06	-1.08	1.39	1.34	0.39	0.36	0.28	0.31	1.62	-1.35
Fe	-0.85	-1.08	-1.08	1.31	1.67	0.44	0.47	0.37	0.39	1.62	-1.36
Cu	-0.06	-1.05	-1.09	2.14	0.85	0.27	0.31	-0.01	0.28	1.54	-0.24
Ga	-1.02	-1.14	-1.09	1.21	2.10	0.60	0.52	0.51	0.46	1.59	-0.52
Al	-1.51	-1.29	-1.10	0.87	3.93	1.16	0.93	0.88	0.96	1.59	-1.15

*: The atomic number is shown in Figure R2. Mt denotes the sum of charges on the four metal atoms.

ADBS relation for monomolecular reactions

Here we show that for a monomolecular reaction, ADBS relation is equivalent to TSS relation. The barrier E_a is

$$E_a = E^{TS}_{A/slab} - E^{IS}_{A/slab} \quad (S1)$$

$$E^{TS}_{A/slab} = E^0_A + D^{TS}_A + E^0_{slab} + D^{TS}_{slab} + E^{TS}_{A\text{-}slab} \quad (S2)$$

$$E^{IS}_{A/slab} = E^0_A + D^{IS}_A + E^0_{slab} + D^{IS}_{slab} + E^{IS}_{A\text{-}slab} \quad (S3)$$

For the meaning of all the symbols appearing in this section, please refer to the definitions in "ADBS relation for bimolecular reactions". The adsorption energies of A in the IS and TS, E^{IS}_{ads} and E^{TS}_{ads}, are

$$E^{IS}_{ads} = (E^{IS}_{A\text{-}slab} + E^0_A + D^{IS}_A + E^0_{slab} + D^{IS}_{slab}) - (E^0_A + E^0_{slab}) = E^{IS}_{A\text{-}slab} + D^{IS}_A + D^{IS}_{slab} \quad (S4)$$

$$E^{TS}_{ads} = (E^{TS}_{A\text{-}slab} + E^0_A + D^{TS}_A + E^0_{slab} + D^{TS}_{slab}) - (E^0_A + E^0_{slab}) = E^{TS}_{A\text{-}slab} + D^{TS}_A + D^{TS}_{slab} \quad (S5)$$

Substitution of S2 and S3 into S1, one gets

$$E_a = E^{TS}_{A/slab} - E^{IS}_{A/slab} = (E^{TS}_{A\text{-}slab} + D^{TS}_A + D^{TS}_{slab}) - (E^{IS}_{A\text{-}slab} + D^{IS}_A + D^{IS}_{slab}) = E^{TS}_{A\text{-}slab} - E^{IS}_{A\text{-}slab} \quad (S6)$$

If ADBS relation holds true for the reaction, then

$$E_a = \alpha E^{IS}_{ads} + \beta \quad (S7)$$

From S6 and S7, we have

$$E^{TS}_{ads} - E^{IS}_{ads} = \alpha E^{IS}_{ads} + \beta \quad (S8)$$

$$E^{TS}_{ads} = (\alpha+1)E^{IS}_{ads} + \beta = \alpha' E^{IS}_{ads} + \beta \quad (S9)$$

Equation (S9) is TSS relation.

ADBS relation for bimolecular reactions

Here we show that we show that when certain conditions are satisfied, the ADBS relation for a bimolecular reaction is equivalent to the TSS relation.

The barrier E_a for a bimolecular surface reaction with reactants A and B is the difference between the total energy of the transition state (TS, $E^{TS}_{A+B/slab}$) and initial state (IS, $E^{IS}_{A+B/slab}$):

$$E_a = E^{TS}_{A+B/slab} - E^{IS}_{A+B/slab} \quad (S10)$$

The total energy of IS and TS can be expressed as (S11) and (S12) respectively:

$$E^{IS}_{A+B/slab} = E^0_A + D^{IS}_A + E^0_B + D^{IS}_B + E^0_{slab} + D^{IS}_{slab} + E^{IS}_{A\text{-}slab} + E^{IS}_{B\text{-}slab} + E^{IS}_{A\text{-}B} \quad (S11)$$

$$E^{TS}_{A+B/slab} = E^0_A + D^{TS}_A + E^0_B + D^{TS}_B + E^0_{slab} + D^{TS}_{slab} + E^{TS}_{A\text{-}slab} + E^{TS}_{B\text{-}slab} + E^{TS}_{A\text{-}B} \quad (S12)$$

Here E^0_A, E^0_B and E^0_{slab} are the total energies of the isolated A and B and clean slab. D^{IS}_A/D^{TS}_A, D^{IS}_B/D^{TS}_B and $D^{IS}_{slab}/D^{TS}_{slab}$ are the deformation energies of A, B and slab in the IS and TS structures with respect to the isolated A and B and clean slab. $E^{IS}_{A\text{-}slab}/E^{TS}_{A\text{-}slab}$, $E^{IS}_{B\text{-}slab}/E^{TS}_{B\text{-}slab}$ and $E^{IS}_{A\text{-}B}/E^{TS}_{A\text{-}B}$ refer to the interaction energy between A

or B and slab and between A and B in the IS/TS structures. Fig. S10 illustrates the deformation energy and interaction energy. Substitution of (S14) and (S12) into (S10) yields equation (S13)

$$E_a = (D_A^{TS} - D_A^{IS}) + (D_B^{TS} - D_B^{IS}) + (D_{slab}^{TS} - D_{slab}^{IS}) + (E_{A\text{-}slab}^{TS} - E_{A\text{-}slab}^{IS}) + (E_{B\text{-}slab}^{TS} - E_{B\text{-}slab}^{IS}) + (E_{A\text{-}B}^{TS} - E_{A\text{-}B}^{IS}) \quad (S13)$$

In our case, the two reactants are CO_2 and H atom. Let B represent H atom, we have $D_B^{IS} = D_B^{TS} = 0$. Rearranging (6), we obtain equation (S14):

$$E_a = (E_{A\text{-}B}^{TS} + E_{A\text{-}slab}^{TS} + D_A^{TS}) - (E_{A\text{-}B}^{IS} + E_{A\text{-}slab}^{IS} + D_A^{IS}) + (E_{B\text{-}slab}^{TS} + D_{slab}^{TS}) - (E_{B\text{-}slab}^{IS} + D_{slab}^{IS}) \quad (S14)$$

$$= (E_{A\text{-}B}^{TS} + E_{A\text{-}slab}^{TS} + D_A^{TS}) - (E_{A\text{-}B}^{IS} + E_{A\text{-}slab}^{IS} + D_A^{IS}) + (E_{slab}^{0} + E_B^0 + E_{B\text{-}slab}^{TS} + D_{slab}^{TS}) - (E_{slab}^{0} + E_B^0 + E_{B\text{-}slab}^{IS} + D_{slab}^{IS}) \quad (S14')$$

Note $(E_{slab}^{0} + E_B^0 + E_{B\text{-}slab}^{TS} + D_{slab}^{TS})$ and $(E_{slab}^{0} + E_B^0 + E_{B\text{-}slab}^{IS} + D_{slab}^{IS})$ denote the total energies of the slab with species B on it in the TS and IS respectively. When they are equal, equation (S14') is reduced to (S15):

$$E_a' = (E_{A\text{-}B}^{TS} + E_{A\text{-}slab}^{TS} + D_A^{TS}) - (E_{A\text{-}B}^{IS} + E_{A\text{-}slab}^{IS} + D_A^{IS}) \quad (S15)$$

E_a' indicates the barrier under the condition that $(E_{slab}^{0} + E_B^0 + E_{B\text{-}slab}^{TS} + D_{slab}^{TS})$ equals to $(E_{slab}^{0} + E_B^0 + E_{B\text{-}slab}^{IS} + D_{slab}^{IS})$. It can be shown that equation (S15) is the difference of adsorption energy of reactant A, $E_{ads(A)}$, on the slab with B adsorbed on it in the TS and IS structures. Take $E_{ads(A)}$ for the IS as an example:

$$E_{ads(A)}^{IS} = (E_{A\text{-}slab}^{IS} + E_{B\text{-}slab}^{IS} + E_{A\text{-}B}^{IS} + E_A^0 + D_A^{IS} + E_B^0 + D_B^{IS} + E_{slab}^{0} + D_{slab}^{IS}) - (E_{B\text{-}slab}^{IS} + E_A^0 + E_B^0 + D_B^{IS} + E_{slab}^{0} + D_{slab}^{IS}) = E_{A\text{-}B}^{IS} + E_{A\text{-}slab}^{IS} + D_A^{IS} \quad (S16)$$

With equation (S16), (S15) can be expressed as (S17)

$$E_a' = E_{ads(A)}^{TS} - E_{ads(A)}^{IS} \quad (S17)$$

Equation (S17) shows that for bimolecular reactions, as long as one of the reactants has no deformation energy and $(E_{slab}^{0} + E_B^0 + E_{B\text{-}slab}^{TS} + D_{slab}^{TS})$ and $(E_{slab}^{0} + E_B^0 + E_{B\text{-}slab}^{IS} + D_{slab}^{IS})$ are equal, the barrier is apparently related to the other reactant only. In our case, deformation energy of H is strictly zero. The assumption that $(E_{slab}^{0} + E_B^0 + E_{B\text{-}slab}^{TS} + D_{slab}^{TS})$ equals to $(E_{slab}^{0} + E_B^0 + E_{B\text{-}slab}^{IS} + D_{slab}^{IS})$ is a strong condition.

$$\text{Let } \Delta E = [(E_{slab}^{0} + E_B^0 + E_{B\text{-}slab}^{TS} + D_{slab}^{TS}) - (E_{slab}^{0} + E_B^0 + E_{B\text{-}slab}^{IS} + D_{slab}^{IS})] \quad (S18)$$

ΔE in S18 is in fact the energy difference of the slab with B on it in the TS and the IS. For the twelve systems studied in the present paper the average absolute value of ΔE is 0.28 eV which is close to the DFT accuracy. The small ΔE explains the existence of ADBS relation for the systems. Generally, ΔE is not zero. From (S14'),(S17) and (S18), the general expression for barrier E_a is

$$E_a = E^{TS}_{ads(A)} - E^{IS}_{ads(A)} + \Delta E = E_a' + \Delta E \quad \text{(S19)}$$

Table S5 lists the values for $E^{TS}_{ads(A)}$, $E^{IS}_{ads(A)}$, ΔE and E_a'. The averaged absolute $E^{IS}_{ads(A)}$ is more than three time as large as $E^{TS}_{ads(A)}$ and there is a linear relation between $E^{IS}_{ads(A)}$ and E_a', as shown by equation (20) and Figure S9:

$$E_a' = -0.919 \times E^{IS}_{ads(A)} + 0.230 \qquad R^2 = 0.87 \quad \text{(S20)}$$

The deviation of Co_4/In_2O_3 system from the fitted line in Figure S9 is due to large value of ΔE (see Table S5).

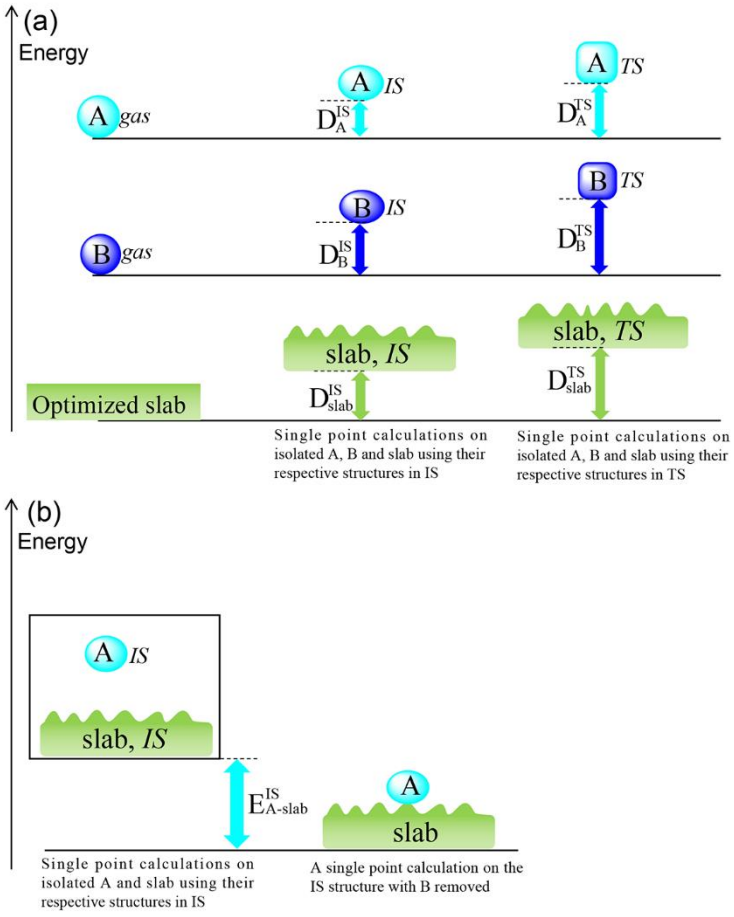

Fig. S10 Illustration of (a) the deformation energy and (b) the interaction energy.

Table S5. Adsorption energies E_{ads} of A (CO_2) with slab plus B (H) in the initial state (IS) and transition state (TS), the energy difference E_a' between $E^{TS}_{ads(A)}$ and $E^{IS}_{ads(A)}$, ΔE, and the calculated barrier E_a.

Systems	$E^{IS}_{ads(A)}$	$E^{TS}_{ads(A)}$	E_a'	ΔE	$E_a' + \Delta E$	E_a
Ag_4/In_2O_3	-0.23	-0.07	0.16	0.24	0.40	0.40
Pt_4/In_2O_3	-0.98	-0.33	0.65	-0.11	0.54	0.55
Pd_4/In_2O_3	-0.94	-0.38	0.56	0.28	0.84	0.84
Rh_4/In_2O_3	-1.61	-0.06	1.55	-0.68	0.87	0.87
Ir_4/In_2O_3	-1.21	-0.07	1.14	-0.10	1.04	1.05

Ni_4/In_2O_3	-0.71	-0.09	0.62	0.30	0.92	0.92
Cr_4/In_2O_3	-1.53	-0.40	1.13	0.11	1.24	1.24
Fe_4/In_2O_3	-1.36	0.01	1.37	-0.25	1.12	1.12
Co_4/In_2O_3	-1.42	-1.38	0.04	0.98	1.02	1.02
Al_4/In_2O_3	-1.00	-0.33	0.67	0.16	0.83	0.84
Ga_4/In_2O_3	-0.78	-0.41	0.37	0.01	0.38	0.38
Cu_4/In_2O_3	-0.25	-0.04	0.21	0.21	0.42	0.42

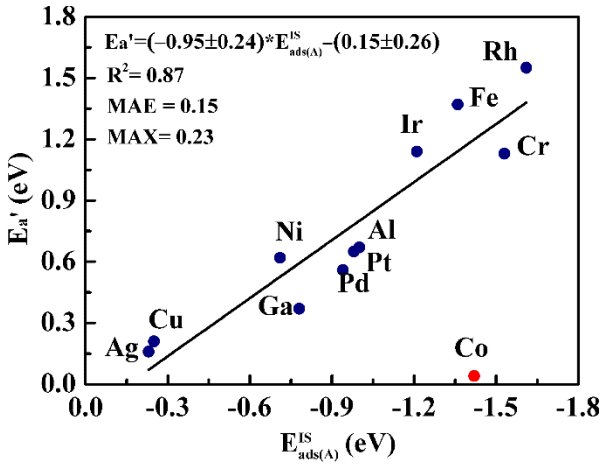

Fig. S11 Liner scaling correlation between the adsorption energy of A (CO_2) on the slab with H adsorbed on it and energy barrier E_a' for CO_2 hydrogenation to HCOO step.

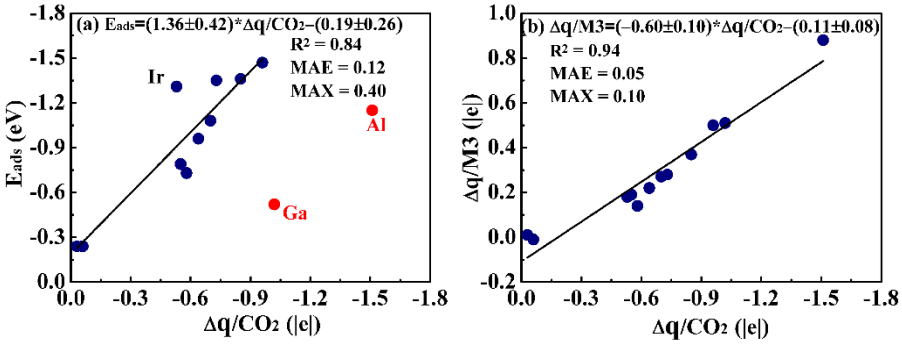

Fig. S12 (a) Correlation between the Bader charges Δq of the CO_2* species and the CO_2 adsorption energies (E_{ads}), and (b) liner scaling correlation between the Bader charges Δq of the CO_2* species and the Bader charges Δq of the M3 atom (see Fig.S13 for M3). The positive/negative value of Δq indicates electron elimination/accumulation, where M = Ag, Pt, Pd, Rh, Ni, Ir, Cr, Co, Fe, Cu, Ga and Al.

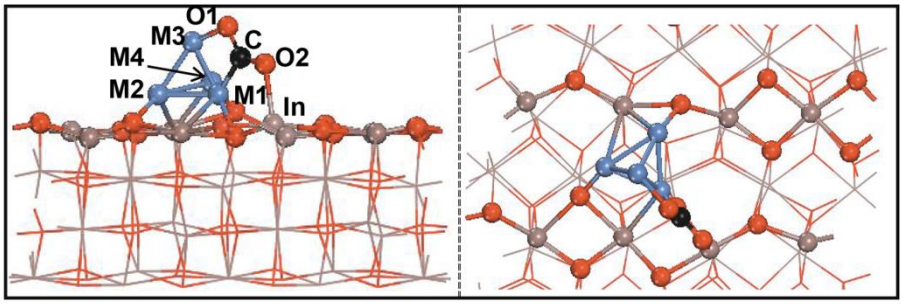

Fig. S13 Optimized adsorbed structure of CO_2 molecular on M_4/In_2O_3 surface, where M = Ag, Pt, Pd, Rh, Ni, Ir, Cr, Co, Fe, Cu, Ga and Al.

R1: $CO_2^* \rightarrow CO^* + O^*$

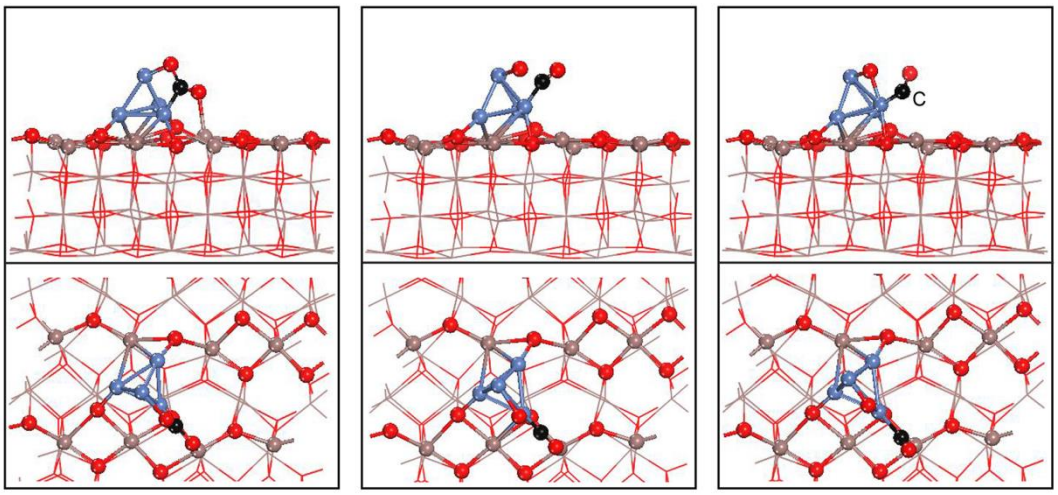

R2: $CO_2^* + H^* \rightarrow trans\text{-}COOH^* + *$

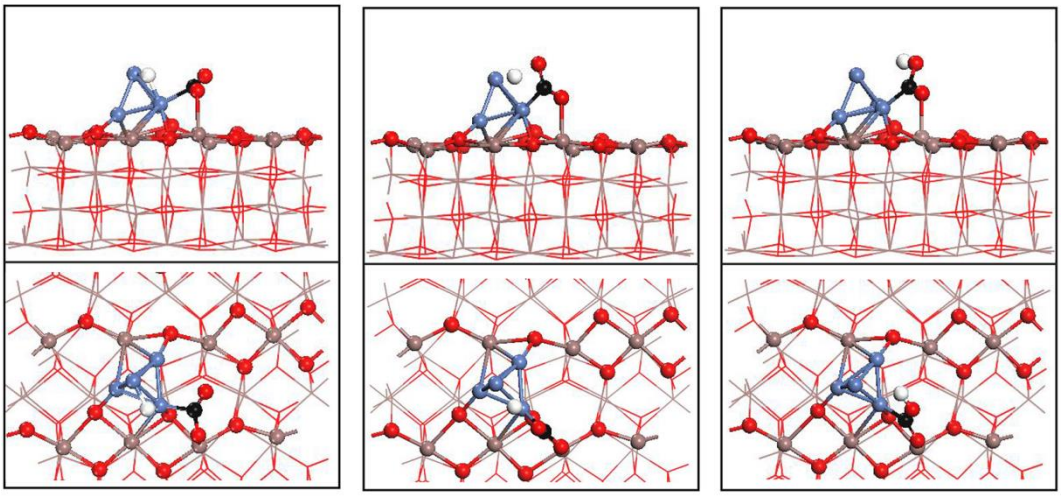

R3: trans-COOH* → cis-COOH*

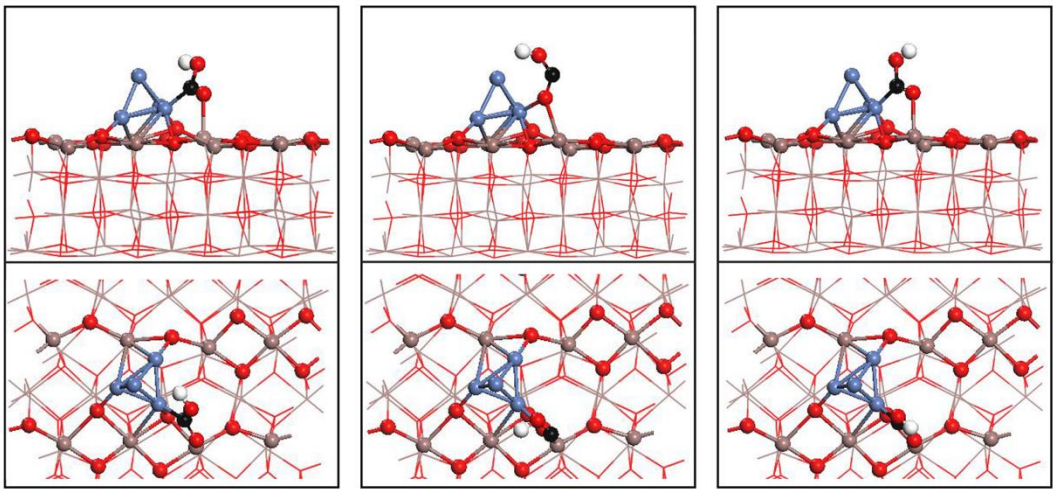

R4: cis-COOH* + H* → CO* + H_2O(g)

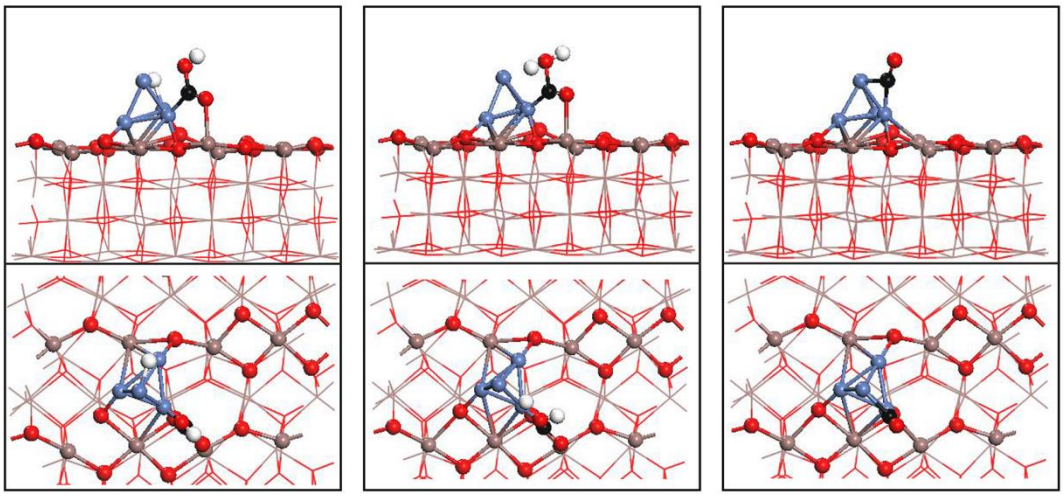

R5: CO_2* + H* → HCOO* + *

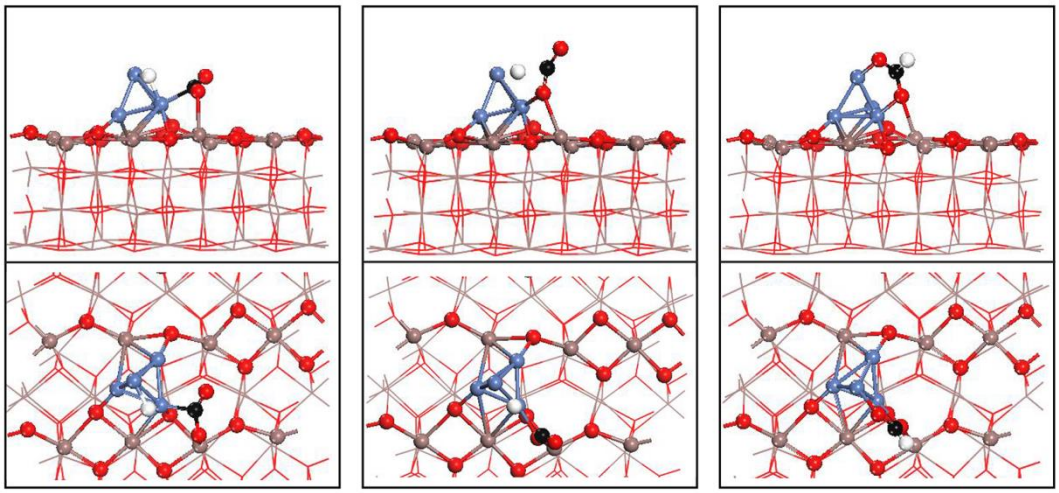

R6: HCOO* + H* → H_2COO* + *

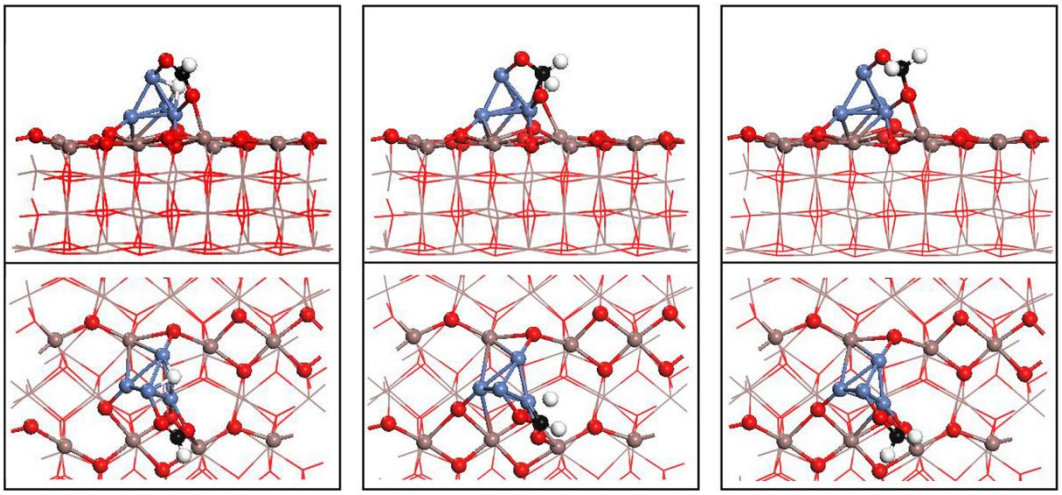

R7: HCOO* + H* → HCOOH* + *

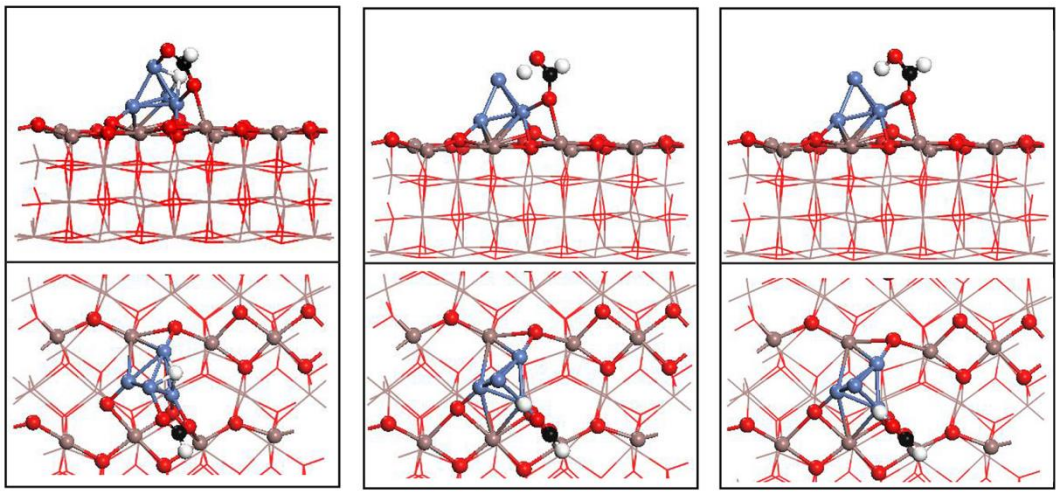

R8: HCOOH* + * →HCO* + OH*

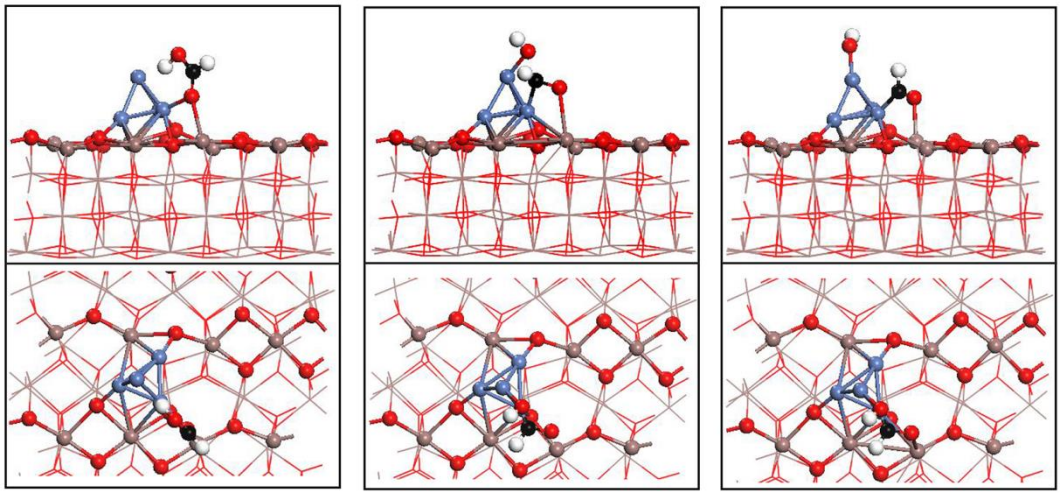

R9: $HCO^* + OH^* + H^* \rightarrow HCO^* + H_2O^* + *$

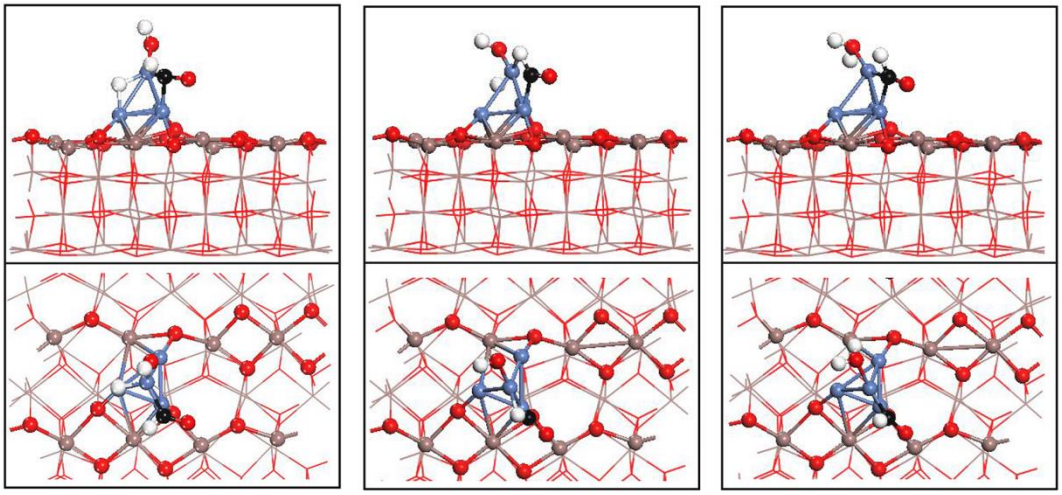

R10: $HCO^* + H^* \rightarrow H_2CO^* + *$

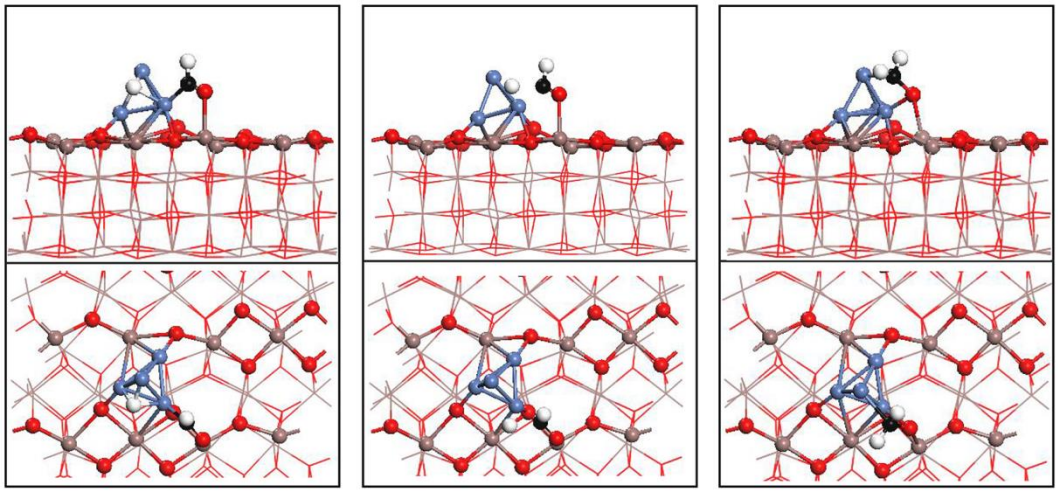

R11: $H_2CO^* + H^* \rightarrow H_3CO^* + *$

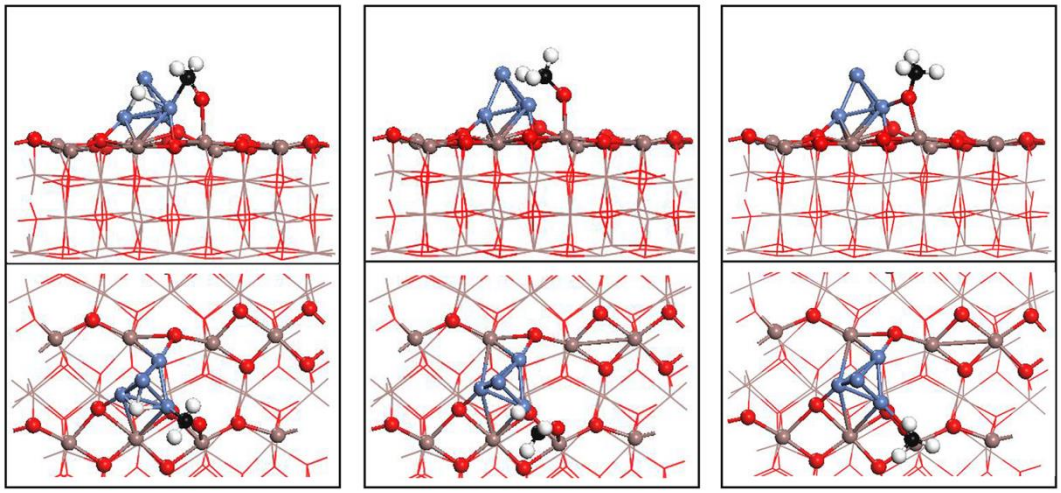

R12: $H_3CO^* + H^* \rightarrow H_3COH^* + *$

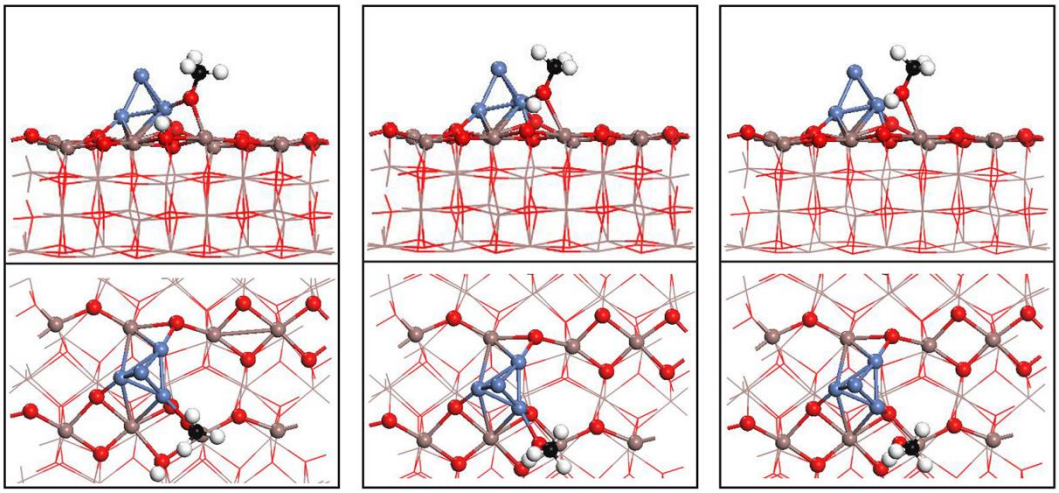

R13: $H_2CO^* + H^* \rightarrow H_2COH^* + *$

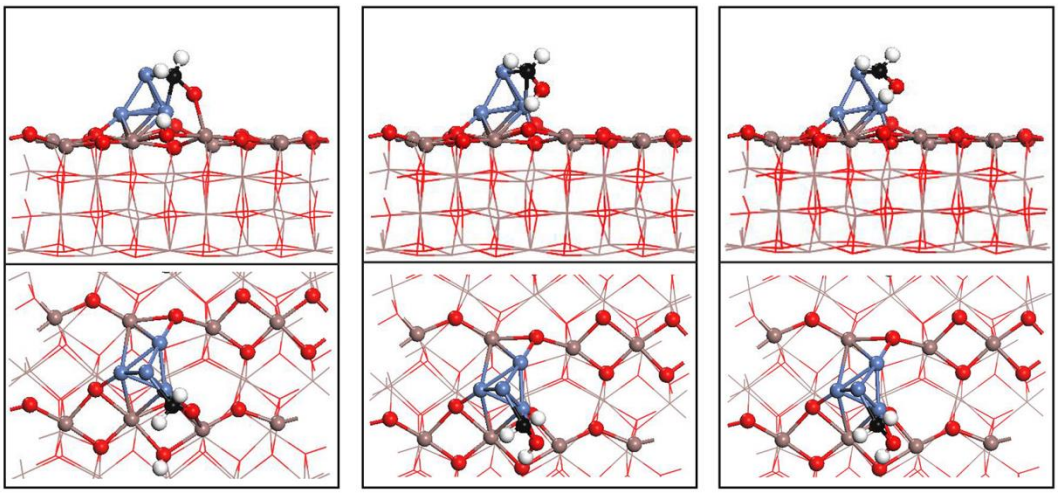

R14: $H_2COH^* + H^* \rightarrow H_3COH^* + *$

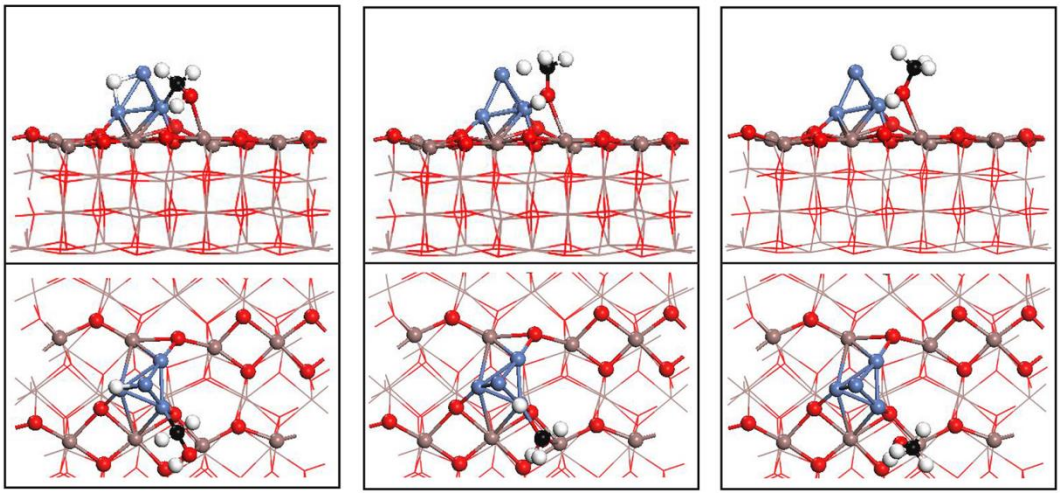

Fig. S14 Illustration of the initial state (left panels), transition state (middle panels) and final state (right panels) for each of elementary steps over $Ni_4/In_2O_3(110)$. Red, O atoms; black, C atoms; white, H atoms; Brown, In atoms; Blue, Ni atoms.

Ag_4/In_2O_3: $CO_2^* + H^* \rightarrow HCOO^* + *$

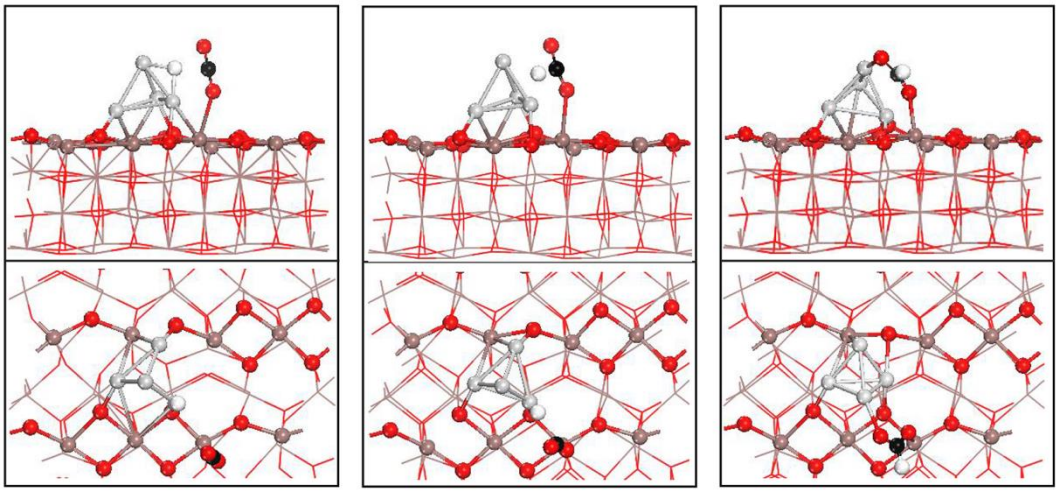

Pt_4/In_2O_3: $CO_2^* + H^* \rightarrow HCOO^* + *$

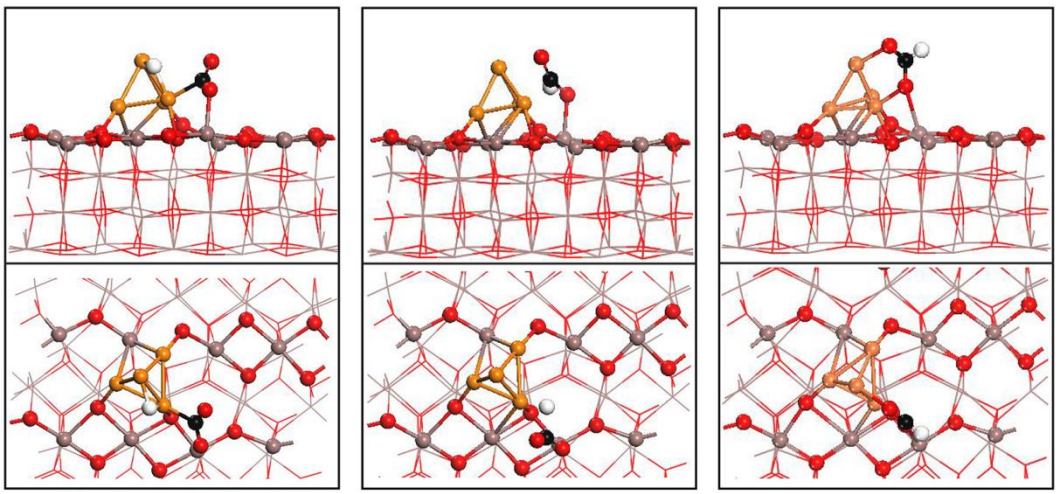

Pd_4/In_2O_3: $CO_2^* + H^* \rightarrow HCOO^* + *$

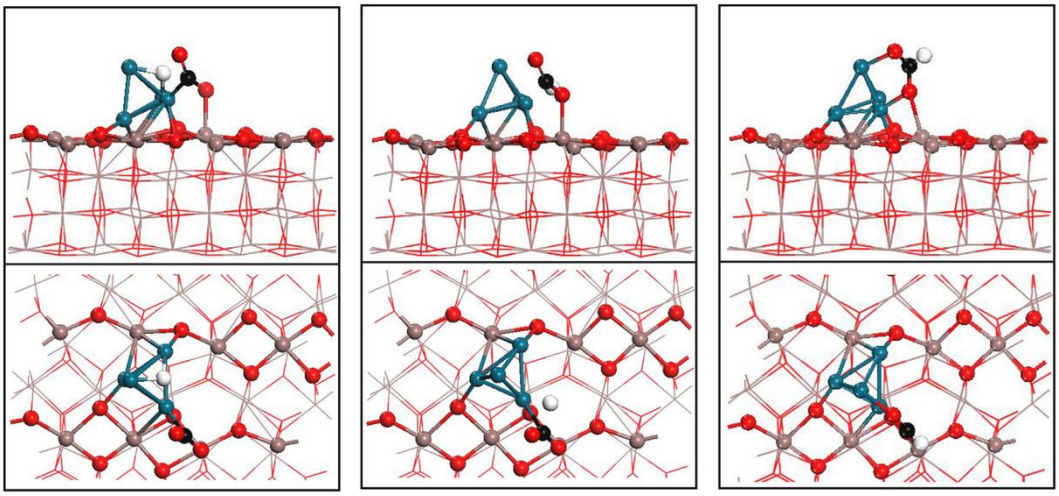

Rh_4/In_2O_3: CO_2* + H* → HCOO* + *

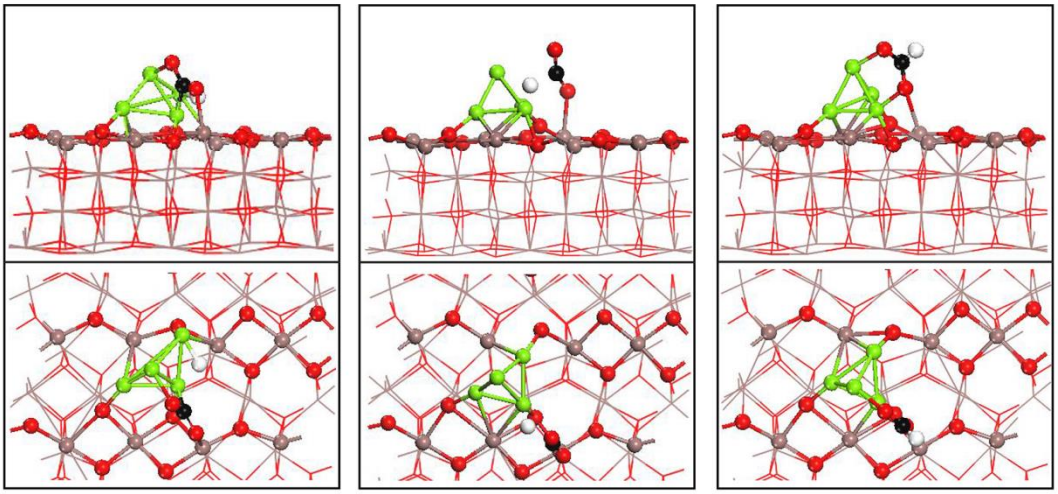

Ir_4/In_2O_3: CO_2* + H* → HCOO* + *

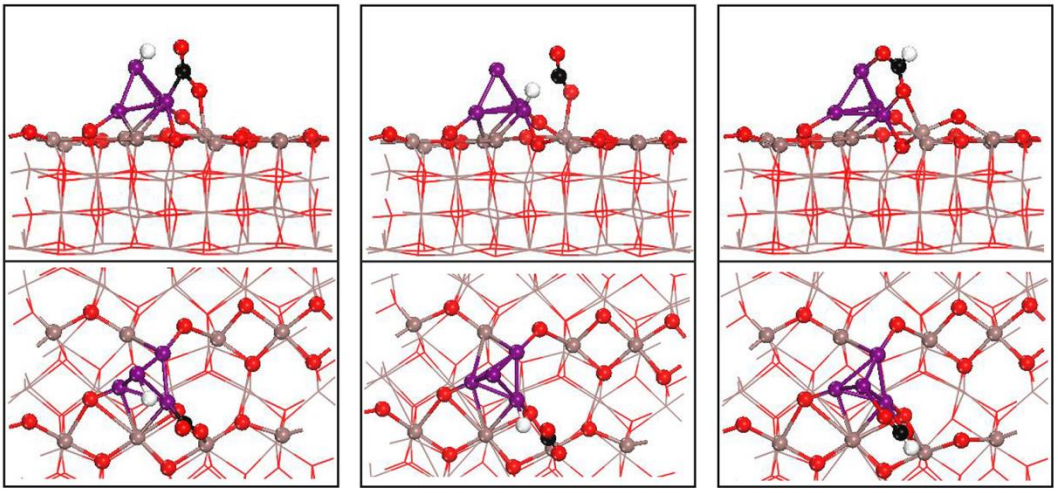

Cu_4/In_2O_3: CO_2* + H* → HCOO* + *

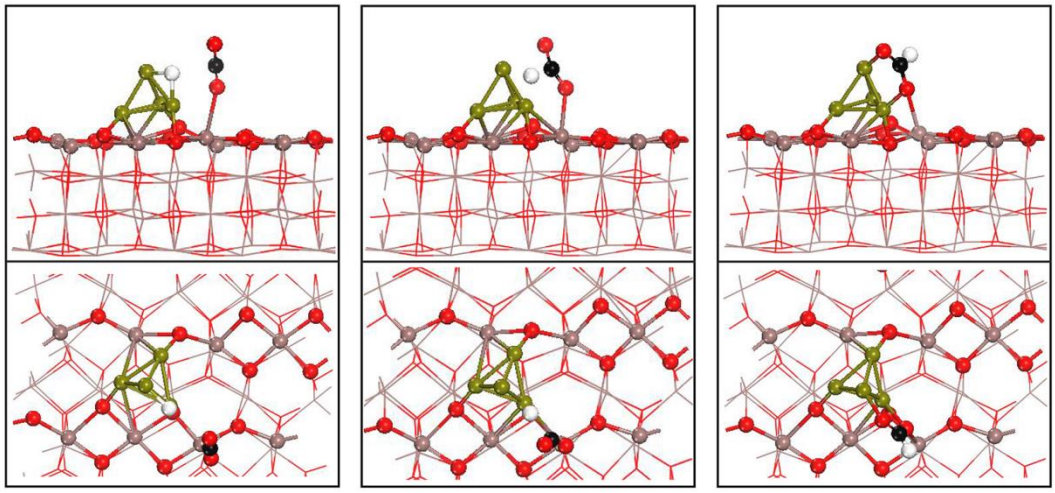

Ga_4/In_2O_3: CO_2* + H* → HCOO* + *

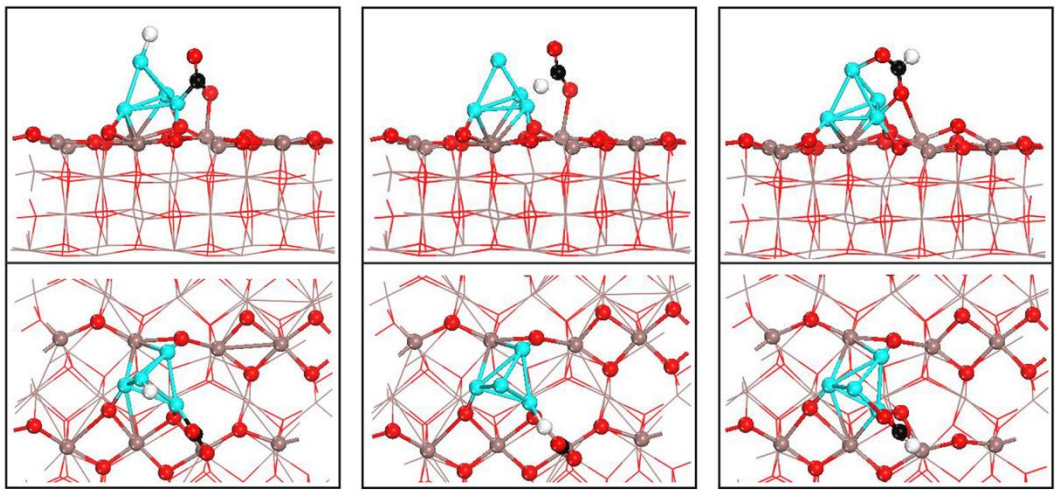

Al_4/In_2O_3: CO_2* + H* → HCOO* + *

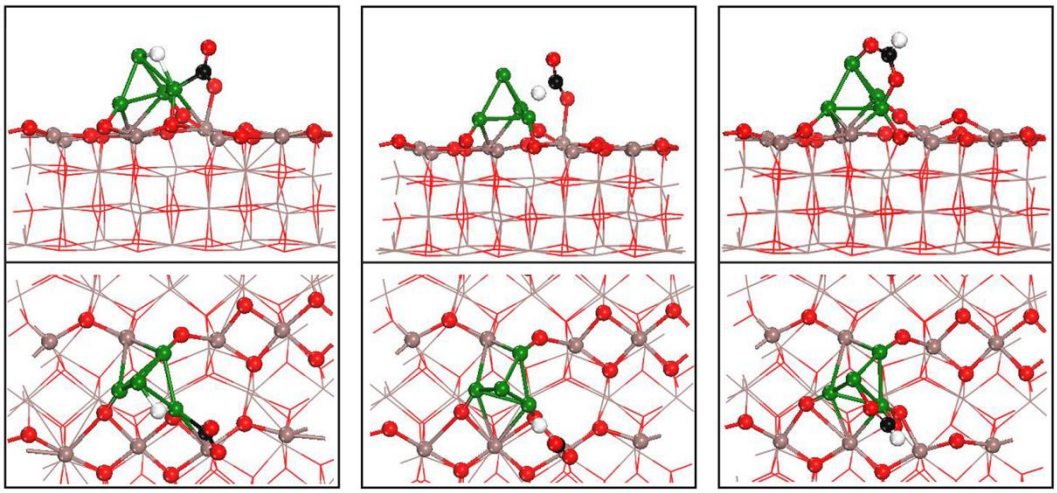

Co_4/In_2O_3: CO_2* + H* → HCOO* + *

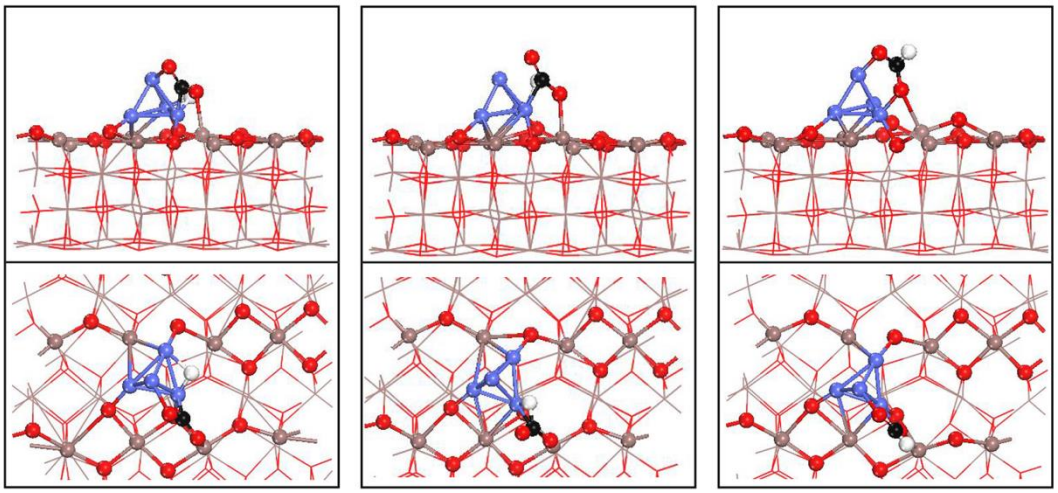

Fe_4/In_2O_3: CO_2* + H* → HCOO* + *

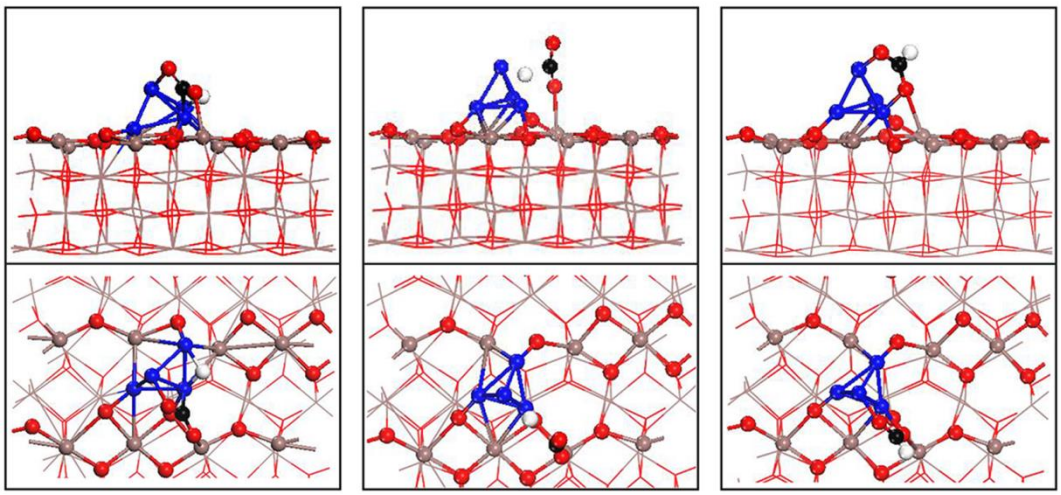

Cr_4/In_2O_3: CO_2* + H* → HCOO* + *

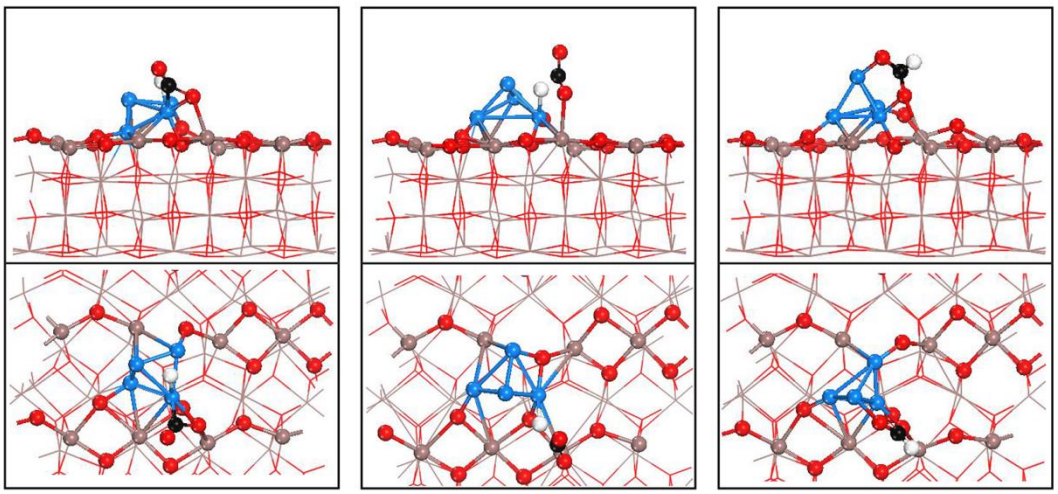

Fig. S15 Illustration of the initial state (left panels), transition state (middle panels) and final

state (right panels) for CO_2* + H* → HCOO* + * step over $M_4/In_2O_3(110)$, where M = Ag, Pt, Pd, Rh, Ir, Cu, Ga, Al, Co, Fe and Cr, respectively.

Reference:

[S1] (a) J. Ye, C. Liu, D. Mei and Q. Ge, *J. Catal*., 2014, **317**, 44−53; (b) N. Rui, K. Sun, C. Shen and C. Liu, *J. CO_2 Util*., 2020, **42**, 101313; (c) K. Sun, N. Rui, C. Shen and C. Liu, *J. Phys. Chem. C*, 2021, **125**, 10926−10936; (d) X. Wang, J. Pan, H. Wei, W. Li, J. Zhao and Z. Hu, *Phys. Chem. Chem. Phys*., 2021, **23**, 11557−11567; (e) C. Shen, Q. Bao, W. Xue, K. Sun, Z. Zhang, X. Jia, D. Mei and C. Liu, *J. Energy Chem.*, 2022**, 65**, 623−629.

[S2] M. Marezio, *Acta Cryst.,* 1966, **20**, 723−728.

[S3] (a) G. Kresse, J. Hafner, *Phys. Rev. B: Condens. Matter Mater. Phys*., 1993, **47**, 558−561; (b) G. Kresse and J. Furthmüller, *Phys. Rev. B: Condens. Matter Mater. Phys*., 1996, **54**, 11169−11186; (c) G. Kresse and J. Furthmuller, *Comput. Mater. Sci*., 1996, **6**, 15−50.

[S4] (a) G. Kresse and D. Joubert, *Phys. Rev. B: Condens. Matter Mater. Phys*., 1999, **59**, 1758−1775; (b) P. E. Blöchl, *Phys. Rev. B: Condens. Matter Mater. Phys*., 1994, **50**, 17953−17979.

[S5] J. P. Perdew, K. Burke and M. Ernzerhof, *Phys. Rev. Lett*., 1996, **77**, 3865−3868.

[S6] (a) S. Grimme, S. Ehrlich and L. Goerigk, *J. Comput. Chem*., 2011, **32**, 1456−1465; (b) S. Grimme, J. Antony, S. Ehrlich and H. Krieg, *J. Chem. Phys*., 2010, **132**, No. 154104.

[S7] (a) H. J. Monkhorst and J. D. Pack, *Phys. Rev. B,* 1976, **13**, 5188−5192; (b) G. Henkelman, B. P. Uberuaga, H. Jónsson, *J. Chem. Phys*., 2000, **113**, 9901−9904.

[S8] G. Henkelman and H. Jonsson, *J. Chem. Phys*., 2000, **113**, 9978−9985.

[S9] P. Hänggi, P. Talkner and M. Borkovec, *Reviews of modern physics*, 1990, **62**,251−341.

[S10] A. P. J. Jansen, *An Introduction to Kinetic Monte Carlo Simulations of Surface Reactions; Springer*: Berlin, Heidelberg, 2012.

[S11] C. A. Wolcott, A. J. Medford, F. Studt, C. T. Campbell, *J. Catal*. **2015**, *330*, 197−207.

[S12] K. Sun, Z. Zhang, C. Shen, N. Rui and C. Liu, *Green Energy Environ*., 2021, **7***,* 807−817.

[S13] N. Rui, Z. Wang, K. Sun, J. Ye, Q. Ge and C. Liu, *Appl. Catal. B,* 2017, **218**, 488−497.

[S14] J. Wang, K. Sun, X. Jia and C. Liu, *Catal. Today,* 2020, **365**, 341−347.

[S15] C. Shen, K. Sun, Z. Zhang, N. Rui, X. Jia, D. Mei and C. Liu, *ACS Catal*., 2021, **11***,* 4036−4046.

[S16] X. Jia, K. Sun, J. Wang, C. Shen and C. Liu, *J. Energy Chem*., 2020, **50**, 409−415.

[S17] K. Sun, N. Rui, Z. Zhang, Z. Sun, Q. Ge and C. Liu, *Green Chem*., 2020, **22**, 5059−5066.

1

2